European Journal of Nuclear Medicine and Molecular Imaging (2021) 48:2531–2542
https://doi.org/10.1007/s00259-020-05083-4

ORIGINAL ARTICLE

Inflammatory response in lungs and extrapulmonary sites detected by [^{18}F] fluorodeoxyglucose PET/CT in convalescing COVID-19 patients tested negative for coronavirus

Yan Bai[1] · Junling Xu[2] · Lijuan Chen[1] · Chang Fu[2] · Yi Kang[3] · Weifeng Zhang[2] · Georges El Fakhri[4] · Jianqin Gu[5] · Fengmin Shao[6] · Meiyun Wang[1]

Received: 8 May 2020 / Accepted: 19 October 2020 / Published online: 9 January 2021

Abstract

Background The severe acute respiratory syndrome coronavirus 2 (SARS-CoV-2) has resulted in an ongoing global pandemic of coronavirus disease 2019 (COVID-19). The challenges associated with imaging infected patients have resulted, to date, in a paucity of metabolic imaging studies of patients with severe COVID-19 infection. Furthermore, it remains unclear if any abnormal metabolic events are taking place in patients who have recovered from COVID-19.

Purpose To use [^{18}F] fluorodeoxyglucose ([^{18}F] FDG) positron emission tomography/computed tomography (PET/CT) to measure metabolic activity in inflamed organs of patients convalescing post severe COVID-19 infection.

Materials and methods A prospective study was performed in seven convalescing patients who were recovering from severe COVID-19 infection in February 2020. Prior to [^{18}F] FDG PET/CT, all patients had received two consecutive negative results of real-time reverse transcriptase polymerase chain reaction (RT-PCR) for SARS-CoV-2 nucleic acid. Clinical intake including symptoms, treatment, laboratory test results, and follow-up was performed. The PET/CT images of COVID-19 patients were compared to a control group of patients that were matched for age and sex.

Results Residual pulmonary lesions were present in all patients and maximum standard uptake value (SUVmax), average standard uptake value (SUVavg), maximum CT intensity (CTmax), and average CT intensity (CTavg) were all significantly greater than in the control group ($p < 0.01$ for all). In addition, SUVmax and SUVavg were significantly greater in the mediastinal lymph node and liver, and SUVmax was significantly greater in the spleen, of COVID-19 patients compared with controls ($p < 0.05$ for all). For the spleen, SUVmax ($r^2 = 0.863$, $p = 0.003$) and SUVavg ($r^2 = 0.797$, $p = 0.007$) were significantly correlated with blood lymphocyte count, and which was below the normal range in five of the seven (71.4%) patients convalescing post severe COVID-19 infection.

Conclusion [^{18}F] FDG PET/CT quantitative analysis has shown that significant inflammation remained in lungs, mediastinal lymph nodes, spleen, and liver after two consecutive negative RT-PCR tests in patients convalescing post severe COVID-19 infection.

Yan Bai, Junling Xu, Lijuan Chen, Chang Fu, contributed equally to this work; Georges El Fakhri, Jianqin Gu, Fengmin Shao and Meiyun Wang contributed equally to this work.

This article is part of the Topical Collection on Infection and inflammation

✉ Meiyun Wang
mywang@ha.edu.cn

[1] Department of Medical Imaging, Henan Provincial People's Hospital & the People's Hospital of Zhengzhou University, No. 7 Weiwu Road, Zhengzhou 450003, Henan, China

[2] Department of Nuclear Medicine, Henan Provincial People's Hospital & the People's Hospital of Zhengzhou University, No. 7 Weiwu Road, Zhengzhou 450003, Henan, China

[3] Department of Infectious Diseases, Henan Provincial People's Hospital & the People's Hospital of Zhengzhou University, No. 7 Weiwu Road, Zhengzhou 450003, Henan, China

[4] Gordon Center for Medical Imaging, Massachusetts General Hospital, Harvard Medical School, 55 Fruit Street, Boston, MA 02114, USA

[5] Department of General Practice, Henan Provincial People's Hospital & the People's Hospital of Zhengzhou University, No. 7 Weiwu Road, Zhengzhou 450003, Henan, China

[6] Department of Nephrology, Henan Provincial People's Hospital & the People's Hospital of Zhengzhou University, No. 7 Weiwu Road, Zhengzhou 450003, Henan, China

Keywords Coronavirus disease 2019 · Severe acute respiratory syndrome coronavirus 2 · PET/CT · [^{18}F] Fluorodeoxyglucose

Introduction

The severe acute respiratory syndrome coronavirus 2 (SARS-CoV-2) has caused an ongoing global pandemic of coronavirus disease 2019 (COVID-19) [1]. As of October 8, 2020, the World Health Organization (WHO) reported that COVID-19 was confirmed in more than 200 countries with a total number of 36,002,827 cases. In a study including a large number of patients, it was reported that over 15% of cases of COVID-19 are classified as severe [2], and in these cases, the mortality at 28 days has been reported to be 61.5% [3], which is similar to that for severe acute respiratory distress syndrome [3, 4].

The epidemiology, clinical characteristics, results of standard clinical laboratory tests, lung appearance on CT, treatment strategies, and outcome in patients with severe COVID-19 have been reported in previous studies [5–9]. Although the SARS-CoV-2 virus has been shown to infect organs other than the lung, such as mediastinal lymph nodes, spleen, and liver [10, 11], quantitative studies of whether this is also the case in patients with COVID-19 are scarce. Such information can be obtained by using [^{18}F] fluorodeoxyglucose ([^{18}F] FDG) positron emission tomography/computed tomography (PET/CT) which is commonly used to evaluate inflammatory and infectious lung diseases [12, 13]. In a retrospective study, Qin et al. reported that four patients with suspected COVID-19 were found to have high uptake of [^{18}F] FDG in pulmonary lesions and mediastinal lymph nodes [14]. However, there have been no reports of the use of [^{18}F] FDG PET/CT in the investigation of patients convalescing post severe COVID-19 infection. Therefore, the objective of the present study was to use [^{18}F] FDG PET/CT to measure metabolic activity throughout the body, and especially lung, mediastinal lymph node, spleen, liver, left ventricular lateral wall, small intestine wall, left and right renal cortex, and brain, of patients convalescing following severe COVID-19 infection in order to shed light on the processes involved in recovery.

Materials and methods

Study participants

This study was carried out at Henan Provincial People's Hospital, Zhengzhou, Henan Province, China, a large hospital designated for use in the treatment of patients with COVID-19. In February 2020, seven patients with severe COVID-19 (3 males, 4 females; age range 56–88 years; mean age 66 years) confirmed by positive RT-PCR test for SARS-CoV-2 were prospectively recruited and enrolled in the study. In addition, a control group of seven age- and sex-matched controls (3 males, 4 females; age range 48–84 years; mean age 65 years) was enrolled in this study. The control group consisted of healthy volunteers without laboratory tests. They were retrospectively selected over the time range of March 2018 to September 2019. Severe patients with COVID-19 were defined according to the seventh edition of the directive "Novel Coronavirus Pneumonia Diagnosis and Treatment Plan" issued by the National Health Commission of China, for COVID-19. To be classified as severe, at least one of the following criteria had to be present: (i) shortness of breath (i.e., respiratory rate ≥ 30 times per minute); (ii) finger blood oxygen saturation ≤ 93%; (iii) arterial partial pressure of oxygen (i.e., inspired oxygen concentration) ≤ 300 mmHg; or (iv) pulmonary lesions increased in size by more than 50% in 24–48 h on lung CT. The study was approved by the local Research Ethics Committee and written informed consent was obtained from all participants.

[^{18}F] FDG PET/CT data acquisition

After confirmation by two consecutive negative results from RT-PCR tests for SARS-CoV-2 nucleic acid that patients were no longer infected with COVID-19, all participants underwent [^{18}F] FDG PET/CT imaging (Discovery VCT, GE Healthcare, Waukesha, WI, USA). Before imaging, all participants fasted for at least 6 h and were confirmed by testing to have a normal blood glucose level. Patients were injected with an intravenous dose of 5.55 mBq per kilogram weight of [^{18}F] FDG. After resting in a dimly lit waiting room for 50 min, PET/CT imaging was performed with coverage from the skull base to mid-thigh. The PET images were acquired with a matrix of 128 × 128 and 3.27-mm slice thickness, and the CT images were acquired with free breathing and with a matrix of 512 × 512 and slice thickness of 3.75 mm at 120 kVp and with a current of 170 mAs.

[^{18}F] FDG PET/CT data processing and analysis

The [^{18}F] FDG PET/CT data was transferred to a computer workstation (GE Healthcare) where the PET and CT images were co-registered and independently analyzed by two radiologists who had over 12 and 21 years of experience, respectively. For each patient, regions of interest (ROIs) were drawn on the CT images of the lung in areas corresponding to where there was obvious loss of aeration together with adjacent areas with normal appearance, as well as in the lung of each control. The short diameter of the mediastinal lymph node was measured on the relevant CT images in both patients and controls.

In addition, the maximum upper and lower, front and rear, and left and right diameters of the lung and spleen were measured on the relevant CT images in patients and controls. ROIs were also drawn on the CT images of the mediastinal lymph nodes with the largest short diameter, and on the sections through the spleen and liver with the largest cross-sectional area in both patients and controls. Finally, for each participant, the ROIs drawn on the CT images were transferred to the co-registered PET images and for each ROI, the maximum standard uptake value (SUVmax) and average standard uptake value (SUVavg) were measured, together with the maximum CT intensity (CTmax) and average CT intensity (CTavg) in Hounsfield units. According to the response, improvement on CT at follow-up was quantified as minimal, partial, significant (only minimal residual), or complete. In addition, the [^{18}F] FDG uptake of the lungs and extrapulmonary sites including mediastinal lymph node, spleen, liver, left ventricular lateral wall, small intestine wall, and left and right renal cortex was compared between those patients who were treated with corticosteroid and those who were not.

Brain PET images were preprocessed and analyzed by using SPM12 (Statistical Parametric Mapping, http://www.fil.ion.ucl.ac.uk/spm/) implemented in Matlab 2012b (MathWorks, Inc.). First, all images were realigned to address any inconsistency in head positioning. Next, a standard PET template was applied to co-register the PET images. Next, the co-registered PET images were normalized to standard Montreal Neurological Institute (MNI) space to remove inter-subject anatomical variability. Smoothing was performed using an isotropic Gaussian filter with a full width at half maximum of 12 mm. Finally, the preprocessed PET images of patients and healthy controls, as well as patients with and without corticosteroid treatment, were compared in a voxel-wise manner based on the framework of the general linear model.

Clinical information and laboratory test results

For each patient, the electronic clinical medical records and results of clinical laboratory tests performed within 5 days before PET/CT imaging were reviewed by a physician who had over 24 years' experience in the treatment of infectious diseases. In addition, RT-PCR tests were performed for each patient to test for SARS-CoV-2 nucleic acid. Smell and taste tests were performed in four patients (patients 4 to 7) at follow-up. In particular, olfactory function was assessed using the smell identification test specifically for the Chinese population, which consists of 40 odor items for testing, and gustatory function was evaluated using the chemotherapy-induced taste alteration scale.

Statistical analysis

Statistical analysis was performed using SPSS 17.0 software (SPSS, Inc., Chicago, IL, USA). The mean results, analyzed by the two radiologists, of each measurement for each participant were used for statistical analyses. The Mann-Whitney *U* test was used to compare the age, SUVmax, SUVavg, CTmax, and CTavg, the largest short diameter of the mediastinal lymph node, as well as the maximum upper and lower, front and rear, and left and right diameters of the spleen, liver, and kidney between patients and controls. [^{18}F] FDG uptake of the lungs and extrapulmonary sites was compared between the patients with and without corticosteroid by using the Mann-Whitney *U* test. A correlation analysis between SUV and CT intensity, as well as between imaging measurements and laboratory test results obtained within 5 days before PET/CT imaging, was performed using Spearman's rank correlation coefficient. A chi-squared test was used to compare the differences in categorical variables. Differences were considered significant for p value < 0.05. For the group analysis of brain PET data, a two-sample t test was used to test for differences in [^{18}F] FDG metabolism ($p < 0.05$, corrected).

Results

Demographic and clinical information for the 7 convalescing COVID-19 patients are presented in Table 1. There was no significant difference in the age distribution of patients and controls ($p = 0.902$). At admission, all patients had fever or respiratory symptoms, but no symptoms of central nervous system (CNS) abnormalities. The patients receive Doxygen therapy, antiviral treatment with lopinavir-ritonavir, arbidol or chloroquine phosphate, as well as anti-inflammatory treatment when necessary. Only patient 1 had diarrhea at admission, which persisted for 3 days, and was not present at the time of PET/CT scanning 19 days after admission. Moreover, there was no abnormal imaging finding in the PET/CT images of the bowel for this patient. No patient was transferred to the intensive care unit and mechanical ventilation was not performed in any patient included in the study. Furthermore, in all patients, the oxygen saturation of blood was below the normal range at admission but increased to normal levels on the day of the PET/CT investigation. The average length of stay of the patients in hospital was 17 days with a range of 11 to 33 days.

[^{18}F] FDG PET/CT images of the lung (panels (A1) to (C1)), mediastinal lymph node (panels (D1) to (F1)), and liver and spleen (panels (G1) to (I1)) in a patient convalescing post severe COVID-19 infection and a matched control subject are shown side by side in Fig. 1. Values of SUVmax, SUVavg, CTmax, and CTavg in the residual pulmonary lesion, adjacent normal-appearing lung tissue, mediastinal lymph node, spleen, liver, left ventricular lateral wall, small intestine wall, left and right renal cortex in patients, and corresponding relevant ROIs in controls are plotted in Fig. 2.

Table 1 Demographic and clinical information for the seven COVID-19 patients

	Patient 1	Patient 2	Patient 3	Patient 4	Patient 5	Patient 6	Patient 7
Basic information							
Age (years)	88	77	79	56	57	59	48
Sex	Female	Male	Female	Female	Male	Male	Female
Date of symptoms onset	Feb. 03	Jan. 20	Feb. 04	Feb. 07	Jan. 27	Feb. 02	Feb. 06
Days between symptoms onset and admission	4	5	0	10	17	5	1
Days between symptoms onset and fever subsided	21	33	18	15	29	22	10
Total hospitalized days	20	33	22	11	15	20	20
Days between symptoms onset and PET scanning	23	37	22	20	31	24	20
Comorbidities							
Hypertension	(−)	(+)	(−)	(−)	(−)	(+)	(−)
Diabetes mellitus	(−)	(−)	(−)	(−)	(−)	(−)	(−)
Cardiovascular disease	(−)	(−)	(+)	(+)	(−)	(−)	(−)
Hyperlipidemia	(−)	(−)	(−)	(−)	(−)	(−)	(−)
Chronic obstructive pulmonary disease	(−)	(+)	(−)	(−)	(−)	(−)	(−)
Oncological disease	(−)	(−)	(−)	(−)	(−)	(−)	(−)
Clinical characteristics at admission							
Maximum temperature (°C)	38.1	36.8	38.5	38.5	38.5	40.0	38.5
Sore throat	(+)	(−)	(−)	(−)	(−)	(−)	(−)
Cough	(−)	(+)	(+)	(+)	(+)	(+)	(+)
Diarrhea	(+)	(−)	(−)	(−)	(−)	(−)	(−)
Sputum	(−)	(+)	(−)	(+)	(−)	(+)	(+)
Shiver	(+)	(−)	(−)	(+)	(+)	(−)	(−)
Fatigue and muscle soreness	(−)	(−)	(−)	(+)	(+)	(−)	(+)
Nausea and vomiting	(−)	(−)	(−)	(−)	(−)	(−)	(−)
Poor appetite	(−)	(+)	(−)	(+)	(+)	(−)	(+)
Headache	(−)	(−)	(−)	(+)	(+)	(−)	(−)
Chest tightness	(−)	(+)	(+)	(+)	(+)	(+)	(+)
Chest pain	(−)	(−)	(−)	(−)	(−)	(−)	(−)
Palpitations	(−)	(+)	(−)	(−)	(−)	(+)	(−)
Shortness of breath	(−)	(+)	(−)	(−)	(−)	(−)	(+)
Oxygen saturation of blood at admission (%)	88	93	91	93	93	91	92
Oxygen saturation of blood at the day of PET/CT scan (%)	98	98	100	98	99	100	99

(+), positive; (−), negative

Residual pulmonary lesions can be seen in the PET/CT image in panels (A1) to (C1) of Fig. 1. On average, in the 7 convalescing COVID-19 patients, these lesions displayed increased SUVmax (mean ± standard deviation, 3.44 ± 2.03 vs 0.54 ± 0.19, $p < 0.01$), SUVavg (2.55 ± 1.24 vs 0.40 ± 0.18, $p < 0.01$), CTmax (42.63 ± 112.80 vs − 477.85 ± 204.06, $p < 0.01$), and CTavg (55.98 ± 148.10 vs − 753.97 ± 96.19, $p < 0.01$) compared with the lungs of controls (Fig. 1, panels (A2) to (C2)). In addition, SUVmax (3.60 ± 0.62 vs 0.54 ± 0.19, $p = 0.01$) and SUVavg (0.98 ± 0.49 vs 0.40 ± 0.18, $p = 0.002$) in the ROI drawn on the CT image in lung tissue adjacent to the pulmonary lesion, and which appeared normal, were also significantly increased compared with the lungs of controls. However, CTmax (− 472.28 ± 105.69 vs − 477.85 ± 204.06, $p = 0.902$) and CTavg (− 733.36 ± 105.69 vs − 753.97 ± 96.19, $p = 0.805$) were not significantly increased in normal-appearing lung tissue relative to the lungs of control subjects.

The mediastinal lymph nodes of the 7 convalescing COVID-19 patients on average showed increased SUVmax (3.60 ± 1.66

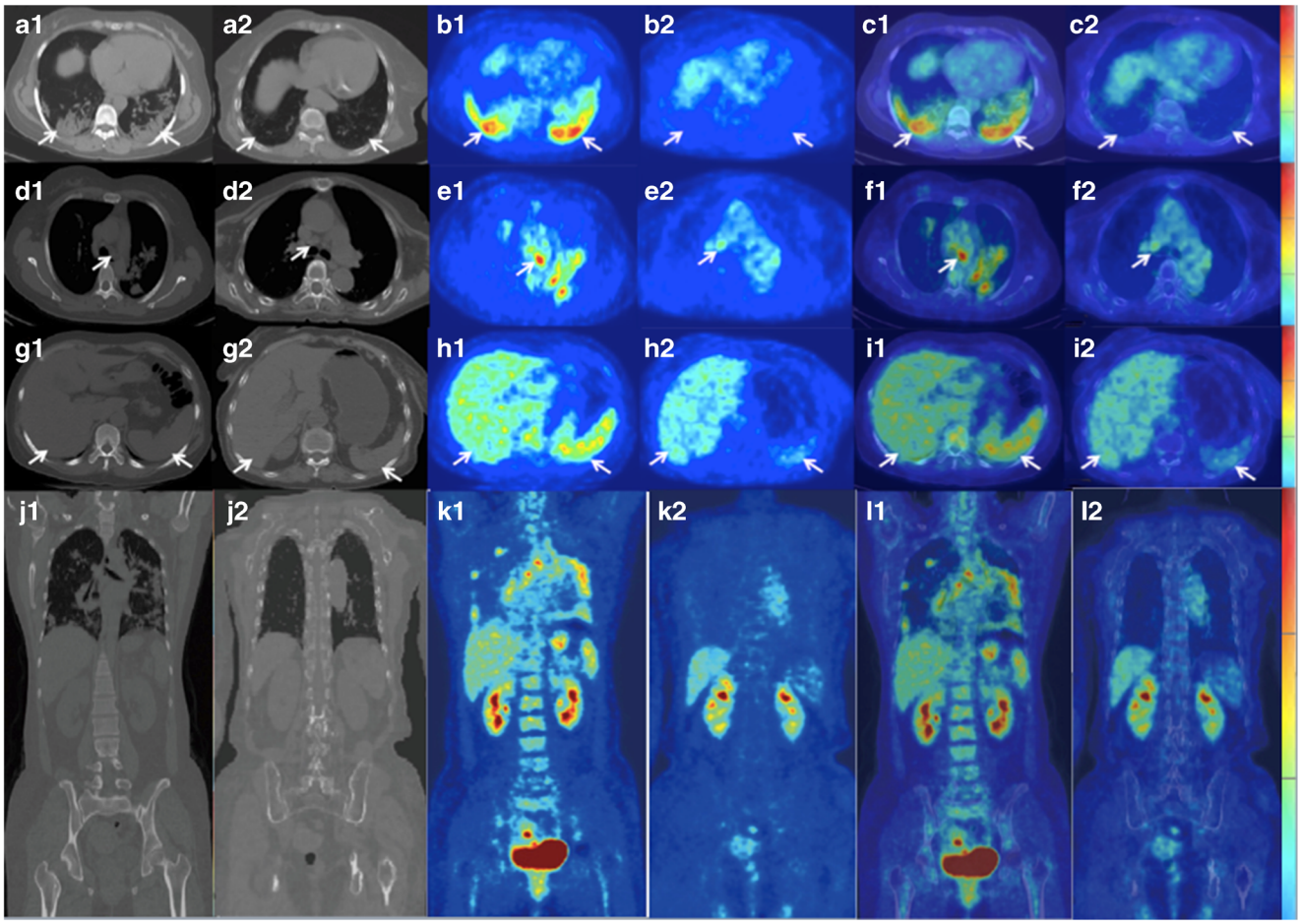

Fig. 1 PET/CT images of a patient (A1–L1) and a control subject (A2–L2). The first and second, third and fourth, and fifth and sixth columns refer to CT, PET, and fused PET/CT images, respectively. The chest CT image shows consolidations in the bilateral lower lungs (A1, arrows; CTmax, 72, CTavg, 18) and the corresponding chest PET image shows increased [^{18}F] fluorodeoxyglucose ([^{18}F] FDG) uptake in the residual pulmonary lesions (B1, arrows; SUVmax, 6.1, SUVavg, 3.8). Lung PET/CT fusion image (C1). The mediastinum CT image shows a normal mediastinal lymph node (D1, arrow; CTmax, 56, CTavg, 24; short diameter, 7 mm). However, the corresponding mediastinum PET image shows increased [^{18}F] FDG uptake in the mediastinal lymph node (E1, arrow; SUVmax, 5.9, SUVavg, 4.6); mediastinum PET/CT fusion image (F1). The abdominal CT image shows a normal spleen and liver (G1, arrows; spleen, CTmax, 102, CTavg, 46; liver, CTmax, 131, CTavg, 51). However, the corresponding abdominal PET image shows increased [^{18}F] FDG uptake in spleen and liver (H1, arrows; spleen, SUVmax, 4.8, SUVavg, 3.0; liver, SUVmax, 4.6, SUVavg, 2.8). The abdomen PET/CT fusion image is also shown (I1), as are the coronal CT (J1), PET (K1), and fused PET/CT (L1) images. In the control subject, the chest CT image shows normal bilateral lungs (A2, arrows; CTmax, − 299, CTavg, − 569) and the chest PET image shows no increased [^{18}F] FDG uptake in the bilateral lungs (B2, arrows; SUVmax, 0.7, SUVavg, 0.6). Lung PET/CT fusion image (C2). The mediastinum CT image shows a normal mediastinal lymph node (D2, arrow; CTmax, 59, CTavg, 24; short diameter, 8 mm) and the mediastinum PET image shows no increased [^{18}F] FDG uptake in the mediastinal lymph node (E2, arrow; SUVmax, 2.2, SUVavg, 2.1). Mediastinum PET/CT fusion image (F2). The abdominal CT image shows a normal spleen and liver (G2, arrows; spleen, CTmax, 93, CTavg, 47; liver, CTmax, 104, CTavg, 56) and the abdominal PET image shows no increased [^{18}F] FDG uptake in the spleen or liver (H2, arrows; spleen, SUVmax, 2.2, SUVavg, 1.7; liver, SUVmax, 3.0, SUVavg, 2.3). Abdomen PET/CT fusion image (I2) is also shown, as are the coronal CT (J2), PET (K2), and fused PET/CT (L2) images

vs ± 1.44 ± 0.57, $p = 0.026$) and SUVavg (2.89 ± 1.14 vs 1.35 ± 0.55, $p = 0.017$) compared with controls. However, as was the case for the normal-appearing lung tissue, there was no significant difference between COVID-19 patients and controls in CTmax and CTavg in the mediastinal lymph nodes (CTmax, 68.85 ± 16.56 vs 40.59 ± 37.23, $p = 0.105$; CTavg, 25.45 ± 15.23 vs 6.96 ± 25.44, $p = 0.165$).

For the liver, SUVmax (4.31 ± 0.91 vs 2.86 ± 0.66, $p = 0.017$) and SUVavg (3.06 ± 0.68 vs 2.25 ± 0.51, $p = 0.038$) were significantly higher in the convalescing COVID-19 patients than in the controls, while for the spleen, only SUVmax (3.31 ± 0.92 vs 2.20 ± 0.53, $p = 0.017$) was significantly higher in the convalescing COVID-19 patients than in the controls. SUVavg (2.27 ± 0.73 vs 1.74 ± 0.38, $p = 0.064$) in the spleen, and CTmax and CTavg in the liver (CTmax, 110.57 ± 15.28 vs 97.85 ± 4.56, $p = 0.068$; CTavg, 59.01 ± 5.99 vs 57.96 ± 4.39, $p = 0.228$) and spleen (CTmax, 93.14 ± 10.80 vs 86.28 ± 7.73, $p = 0.122$; CTavg, 48.03 ± 4.91 vs 50.59 ± 5.38, $p = 0.159$) showed no significant difference between COVID-19 patients and controls. SUVmax, SUVavg,

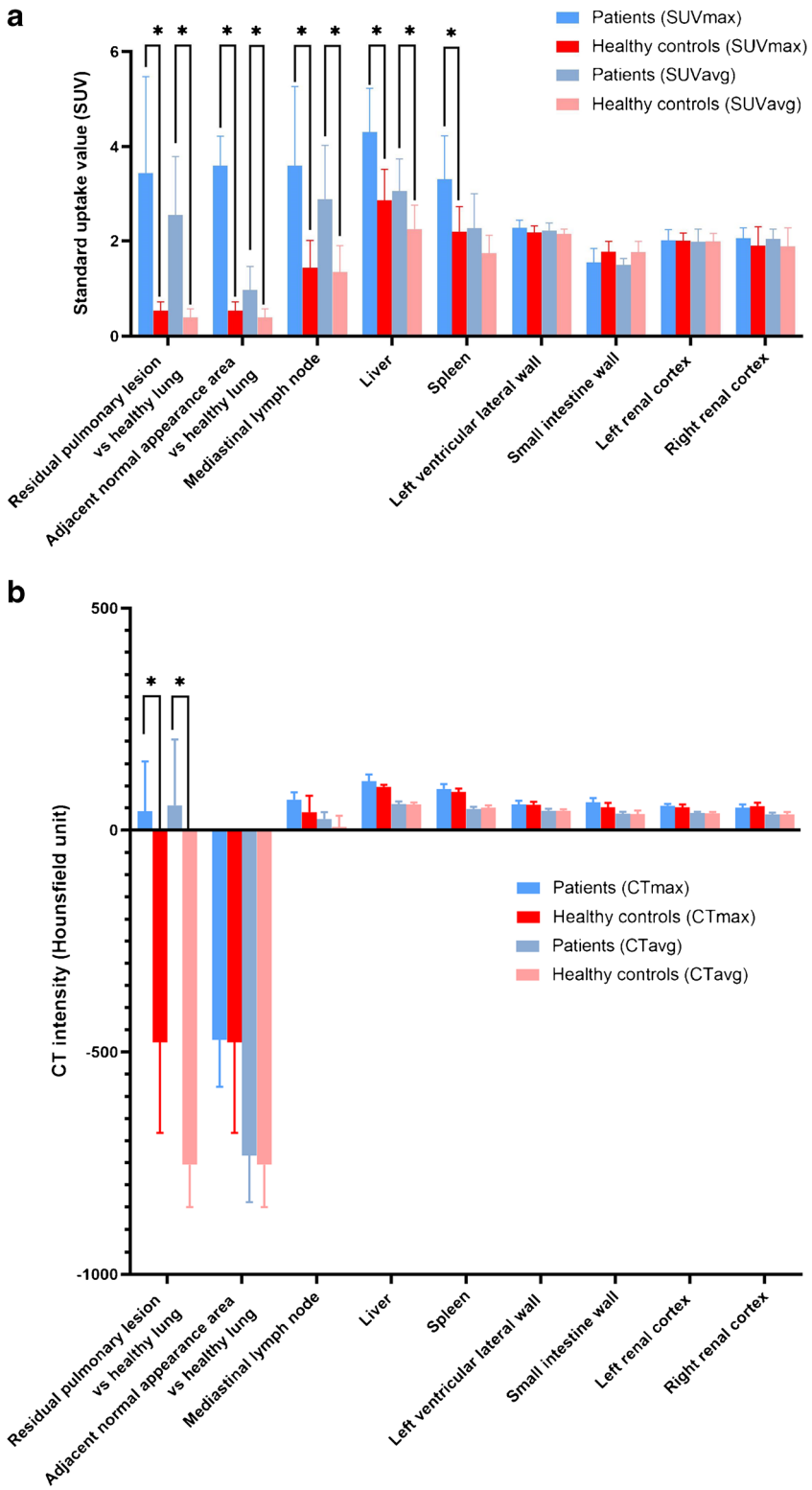

Fig. 2 Graphs of the average values of SUVmax and SUVavg (A) and CTmax and CTavg (B) in ROIs in the residual pulmonary lesion, adjacent normal-appearing lung tissue, mediastinal lymph node, spleen, liver, left ventricular lateral wall, small intestine wall, and left and right renal cortex of the convalescing COVID-19 patients compared with the controls. Error bars represent the standard deviation. Parameters marked with asterisks are significant ($p < 0.05$)

CTmax, and CTavg in the left ventricular lateral wall (SUVmax, 2.28 ± 0.16 vs 2.18 ± 0.14, $p = 0.383$; SUVavg, 2.22 ± 0.15 vs 2.15 ± 0.10, $p = 0.535$; CTmax, 58.14 ± 8.47 vs 57.57 ± 6.32, $p = 0.902$; CTavg, 43.79 ± 4.45 vs 43.79 ± 3.21, $p = 0.710$), small intestine wall (SUVmax, 1.56 ± 0.28 vs 1.77 ± 0.22, $p = 0.128$; SUVavg, 1.50 ± 0.14 vs 1.76 ± 0.23, $p = 0.053$; CTmax 62.71 ± 9.72 vs 51.43 ± 10.13, $p = 0.073$; CTavg 36.93 ± 4.66 vs 36.07 ± 8.28, $p = 0.902$), left renal cortex (SUVmax, 2.01 ± 0.23 vs 2.00 ± 0.17, $p = 0.902$; SUVavg, 1.98 ± 0.27 vs 1.99 ± 0.17, $p = 0.902$; CTmax,

55.00 ± 4.32 vs 51.43 ± 6.55, $p = 0.209$; CTavg, 38.51 ± 2.98 vs 38.03 ± 2.94, $p = 0.902$), and right renal cortex (SUVmax, 2.06 ± 0.22 vs 1.90 ± 0.40, $p = 0.535$; SUVavg, 1.96 ± 0.20 vs 1.88 ± 0.40, $p = 0.535$; CTmax, 50.86 ± 7.17 vs 54.29 ± 7.61, $p = 0.710$; CTavg, 35.49 ± 3.76 vs 35.59 ± 5.29, $p = 0.805$) showed no significant differences between COVID-19 patients and controls. In addition, there were no voxel clusters of statistical significance in the brain PET SUV between COVID-19 patients and controls, as well as the patients with and without corticosteroid ($p > 0.05$, corrected). Moreover, the [^{18}F] FDG uptake of the lungs and extrapulmonary sites had no significant difference between the patients with and without corticosteroid (all $p > 0.05$).

No significant differences were detected in the size of the mediastinal lymph node, spleen, liver, or kidney of the convalescing COVID-19 patients and controls. In particular, the largest short diameter (0.85 ± 0.32 vs 0.60 ± 0.28 cm, $p = 0.221$) of the mediastinal lymph node, as well as the maximum upper and lower (spleen, 9.32 ± 1.66 vs 7.85 ± 1.84 cm, $p = 0.128$; liver, 13.61 ± 2.50 vs 12.71 ± 3.34 cm, $p = 0.456$; left kidney, 10.1 vs 10.1 cm, $p = 0.710$; right kidney, 10.9 vs 11.0 cm, $p = 0.710$), front and rear (spleen, 6.62 ± 2.19 vs 7.04 ± 2.18 cm, $p = 0.710$; liver, 16.34 ± 1.45 vs 15.38 ± 2.25 cm, $p = 0.902$; left kidney, 5.9 vs 5.6 cm, $p = 0.209$; right kidney, 5.7 vs 5.5 cm, $p = 1.000$), and left and right (spleen, 8.30 ± 1.11 vs 6.96 ± 1.31 cm, $p = 0.073$; liver, 17.51 ± 2.05 vs 17.72 ± 2.20 cm, $p = 0.535$, left kidney, 5.8 vs 5.8 cm, $p = 0.710$; right kidney, 5.9 vs 5.8 cm, $p = 0.383$) diameters of the spleen and liver were not significantly different between patients and controls.

The result of Spearman's rank correlation analysis revealed that in the residual pulmonary lesion of patients, SUVmax was significantly correlated with CTmax ($r^2 = 0.929$, $p < 0.001$), and SUVavg was significantly correlated with the CTavg ($r^2 = 0.797$, $p < 0.001$). The results of laboratory tests performed for the COVID-19 patients within 5 days of the PET/CT investigation are presented in Table 2.

For the spleen, lymphocyte count in peripheral blood was positively correlated with SUVmax ($r^2 = 0.863$, $p = 0.003$) and SUVavg ($r^2 = 0.797$, $p = 0.007$), but not significantly correlated with CTmax ($r^2 = 0.368$, $p = 0.148$) or CTavg ($r^2 = 0.127$, $p = 0.432$) (Fig. 3 A and B). In addition, C-reactive protein was not significantly correlated with SUVmax ($r^2 = 0.011$, $p = 0.819$), SUVavg ($r^2 = 0.001$, $p = 0.939$), CTmax ($r^2 = 0.184$, $p = 0.337$), or CTavg ($r^2 = 0.081$, $p = 0.535$) in spleen (Fig. 3 C and D). No significant correlations were observed between neutrophil count, procalcitonin, alanine aminotransferase, aspartate aminotransferase, and any of the measures obtained for the ROIs drawn on the PET/CT images (all $p > 0.05$).

Treatment and follow-up information for the COVID-19 patients are presented in Table 3. All patients were discharged 1 to 2 days after [^{18}F] FDG PET/CT scanning. As part of the follow-up, thoracic CT scans were performed in patients 2 to 7 and demonstrated that there had been improvements in the residual pulmonary lesions. According to the improvement on CT images at follow-up, the evaluation results were consistent between the two radiologists. Patients 2 and 3 had partial improvement, while patients 4 to 7 had significant improvement on CT images. Additional negative RT-PCR SARS-CoV-2 nucleic acid test results were obtained in patients 4 to 7 during follow-up. Follow-up also confirmed that all patients' respiratory symptoms steadily after discharge. In 4 patients (patients 3 to 6), light respiratory symptoms (mild cough) persisted at follow-up; however, no relationship was found between the respiratory symptoms and residual consolidation ($p = 0.43$) or fibrosis ($p = 0.54$) on CT images. The olfactory function in three (patients 4 to 6) of four patients (75%) was mildly abnormal. The taste test results were normal in all of the four patients who were tested. The average intraclass correlation coefficient between the two radiologists for all the measures was 0.84.

Discussion

This is a study reporting the use of [^{18}F] FDG PET/CT to measure metabolism of lung and other organs in patients convalescing after severe COVID-19 infection. Although the patients had two consecutive negative results of RT-PCR tests for SARS-CoV-2 nucleic acid, [^{18}F] FDG PET/CT imaging revealed increased metabolic activity in residual pulmonary lesions, normal-appearing lung tissue, mediastinal lymph nodes, spleen, and liver. These findings are interpreted as showing that there is persisting inflammation in these tissues and which has lasted beyond the "negative" status conferred by the double RT-PCR testing. This is a key finding that may help shed light on subsequent patho-physiological processes taking place in patients who have recovered.

[^{18}F] FDG PET/CT has previously been used to diagnose and monitor a variety of infectious and inflammatory lung diseases [12]. For example, increased uptake of [^{18}F] FDG in pulmonary lesions has been reported in cases of pneumonia such as influenza A infection, aspiration pneumonia, and organized pneumonia [12, 13]. In addition, a previous PET/CT study by Qin et al. [14] in four patients who were highly suspected of having a COVID-19 infection demonstrated that the pulmonary lesions were characterized by high uptake of [^{18}F] FDG. Recently, Dietz et al. reported increased [^{18}F] FDG uptake in the lung lesions of all thirteen non-critically ill COVID-19 patients between day 6 and day 14 after the onset of symptoms [15]. Moreover, Colandrea et al. reported high [^{18}F] FDG uptake in lung lesions in 4 of 5 (80%) oncological patients without symptoms but with COVID-19 [16]. The results of the present study add to this knowledge by further showing that metabolic activity in residual pulmonary

Table 2 Laboratory test results obtained for the COVID-19 patients before the PET/CT investigation

	Patient 1	Patient 2	Patient 3	Patient 4	Patient 5	Patient 6	Patient 7
Laboratory results (normal range) within 5 days before PET/CT scans							
White blood cell count (3.9–9.9 × 10^9 cells/L)	3.72 (↓)	3.74 (↓)	5.56	5.82	5.73	5.08	11.20 (↑)
Lymphocyte count (1.1–3.2 × 10^9 cells/L)	0.92 (↓)	0.85 (↓)	0.82 (↓)	0.83 (↓)	1.39	0.97 (↓)	1.75
Neutrophil count (1.8–6.3 × 10^9 cells/L);	2.46	4.31	4.27	2.54	3.65	3.67	8.10 (↑)
C-reactive protein (0.0–10 mg/L)	1.1	14.2 (↑)	8.85	1.50	20.2 (↑)	23.80 (↑)	7.80
Procalcitonin (0–0.25 ng/mL)	0.09	0.01	0.05	0.08	0.08	0.02	0.01
Liver function							
Alanine aminotransferase (7–40 U/L)	13.0	18.2	16.0	38.6	20.1	60.0 (↑)	28.10
Aspartate aminotransferase (13–35 U/L)	26.2	28.3	20.2	37.6 (↑)	22.9	33.7	28.8
Renal function							
Urea (2.5–7.1 mmol/L)	4.64	2.94	5.10	4.40	NA	4.64	2.98
Creatinine (44–104 μmol/L)	34 (↓)	53	50	35 (↓)	NA	48	46
Uric acid (155–428 μmol/L)	149.2 (↓)	218.9	248	215.8	NA	177.4	194.3
Retinol binding protein (25–70 mg/L)	24.3 (↓)	17.6 (↓)	25.4	39.5	NA	38.2	38.1
Examinations on heart							
Electrocardiogram	(−)	(−)	(−)	(−)	(−)	(−)	(−)
Echocardiography	(−)	(−)	(−)	(−)	(−)	(−)	(−)

(+), positive; (−), negative; ↑, above normal range; ↓, below normal range

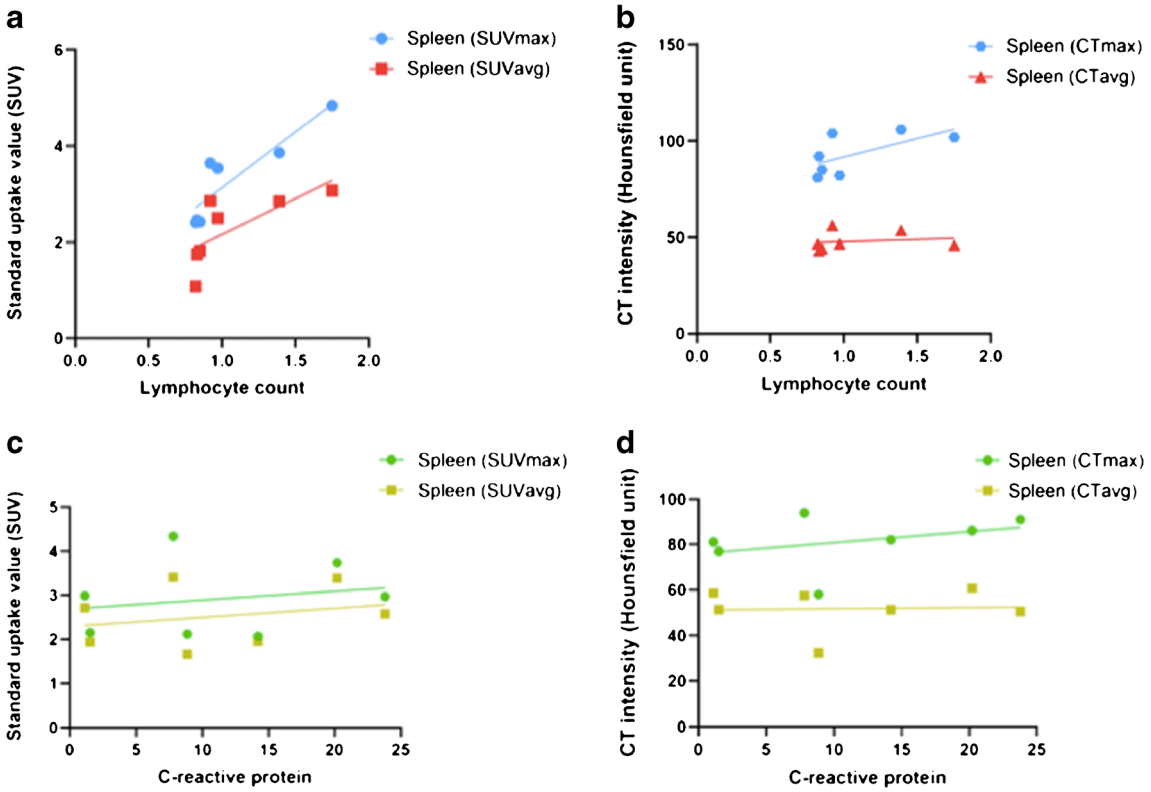

Fig. 3 Correlations between SUVmax, SUVavg, CTmax, and CTavg of spleen and lymphocyte count (A, B) or C-reactive protein (C, D) of peripheral blood in the convalescing COVID-19 patients were assessed using Spearman's rank correlation analyses. The lymphocyte count was strongly correlated with the SUVmax ($r^2 = 0.863$, $p = 0.003$) and SUVavg ($r^2 = 0.797$, $p = 0.007$) (A). However, the lymphocyte count was not significantly correlated with CTmax ($r^2 = 0.368$, $p = 0.148$) or CTavg ($r^2 = 0.127$, $p = 0.432$) (B). The C-reactive protein was not significantly correlated with SUVmax ($r^2 = 0.011$, $p = 0.819$), SUVavg ($r^2 = 0.001$, $p = 0.939$ (C), CTmax ($r^2 = 0.184$, $p = 0.337$), or CTavg ($r^2 = 0.081$, $p = 0.535$) (D)

Table 3 Treatment and follow-up information for the COVID-19 patients

	Patient 1	Patient 2	Patient 3	Patient 4	Patient 5	Patient 6	Patient 7
Treatment							
Oxygen support (nasal cannula)	(+)	(−)	(+)	(+)	(+)	(+)	(+)
Antiviral therapy	(+)	(+)	(+)	(+)	(+)	(+)	(+)
Antibiotic therapy	Levofloxacin	(−)	(−)	Levofloxacin	Levofloxacin	Moxifloxacin Efatriaxone	Moxifloxacin
Traditional Chinese medicine	(+)	(+)	(+)	(+)	(+)	(+)	(+)
Use of corticosteroid	(−)	(−)	(−)	(+)	(+)	(+)	(+)
Follow-up							
Days of follow-up after discharged	19	13	14	15	15	18	19
Improvement on CT images	NA	Partial	Partial	Significant	Significant	Significant	Significant
Residual consolidation on CT images	NA	(−)	(−)	(−)	(−)	(+)	(−)
Residual fibrosis on CT images	NA	(−)	(+)	(−)	(+)	(+)	(+)
SARS-CoV-2 RT-PCR test	NA	NA	NA	(−)	(−)	(−)	(−)
Anosmia	NA	NA	NA	Mild abnormal	Mild abnormal	Mild abnormal	(−)
Ageusia	NA	NA	NA	(−)	(−)	(−)	(−)
Light respiratory symptoms	(−)	(−)	Mild cough	Mild cough	Mild cough	Mild cough	(−)
Central neurological symptoms	(−)	(−)	(−)	(−)	(−)	(−)	(−)
Cardiovascular system symptoms	(−)	(−)	(−)	(−)	(−)	(−)	(−)
Low-grade fever	(−)	(−)	(−)	(−)	(−)	(−)	(−)
Fatigue	(−)	(−)	(−)	(−)	(+)	(−)	(−)
Dermatological lesions	(−)	(−)	(−)	(−)	(−)	(−)	(−)
Gastrointestinal symptoms	(−)	(−)	(−)	(−)	(−)	(−)	(−)

(+), positive; (−), negative; ↑, above normal range; ↓, below normal range, *NA*, not available

lesions remained high even in patients convalescing from COVID-19 who had two consecutive negative RT-PCR test results. This finding is consistent with those of a recent pathology study which found interstitial mononuclear inflammatory infiltrates, dominated by lymphocytes, in both lungs of a patient with COVID-19 [17] and indicates that significant inflammation may persist in the lungs during convalescence. A thoracic CT scan is frequently used to monitor the progression of pulmonary lesions in patients with COVID-19 [10] and the correlation analysis performed in the present study revealed that SUV was positively correlated with CT image intensity in the residual pulmonary lesion. Furthermore, the increase in SUV occurred not only in regions of the lung shown to exhibit loss of aeration but also in adjacent regions of the lung with normal appearance on CT. Bellani et al. [4] reported increased uptake of [^{18}F] FDG in regions of the lung shown to be normally aerated on CT in a patient with influenza A infection. The increased uptake of [^{18}F] FDG could be interpreted as reflecting increased glycolytic activity due to infiltration and inflammation of regions of the lung that would have been considered to be aerated functioning normally if only CT images had been reviewed [18]. Thus, [^{18}F] FDG PET/CT is more sensitive than conventional CT imaging for detecting regions of inflammation in the lung of patients with COVID-19.

The [^{18}F] FDG uptake of the mediastinal lymph node was also higher in patients convalescing after COVID-19 infection than in the control group. This finding is consistent with a previous study in which it was reported that patients who were most highly suspected as having COVID-19 infection had [^{18}F] FDG-avid lymph nodes in the mediastinum [14]. The present study has shown that the short diameter of the mediastinal lymph node was not different between the patients convalescing after COVID-19 and controls, being less than 1 cm in both groups. This finding is consistent with a CT imaging study by Shi et al. [10] who reported that swelling of the lymph node (i.e., lymphadenopathy) was only seen in 13% of patients with COVID-19. Also, these authors reported that the intensity of the mediastinal lymph node on the CT image was not significantly different between the COVID-19 patients and controls. In a previous study by Dietz et al., it was reported that increased uptake of [^{18}F] FDG occurred in the mediastinal lymph node in 100% of COVID-19 patients, while all the short-axis dimensions of mediastinal lymph node were less than 1 cm [15]. Moreover, high [^{18}F] FDG uptake in mediastinal lymph nodes may be secondary to the lung involvement in COVID-19 rather than reflecting new, metastatic disease [19]. Thus, increased [^{18}F] FDG PET/CT metabolic activity together with normal size of the mediastinal lymph node may be a characteristic feature of COVID-19.

The spleen is the largest organ of the lymphatic system [20]. The SUVmax of spleen was increased in patients compared with the control group. In a previous study, CT image intensity of the spleen was not significantly different between COVID-19 patients and controls, whereas measurement of SUVmax by using [^{18}F] FDG PET/CT was shown to be useful for evaluating spleen immune metabolism [21]. In the present study, 71.4% of patients convalescing after COVID-19 infection had decreased lymphocyte count in peripheral blood. Previously, it has been reported that lymphocyte count was decreased in conjunction with a reduction in multiple types of immune cells in the spleen of patients with severe acute respiratory syndrome (SARS), suggesting that immunodeficiency may play an important role in the pathogenesis of SARS [22]. Interestingly, in the present study, lymphocyte count was found to be strongly correlated with SUVmax of the spleen ($r^2 = 0.863$, $p = 0.003$) in patients convalescing after COVID-19 infection. This suggests that increased metabolic activity in the spleen may have produced increased numbers of lymphocytes in peripheral blood. The metabolism of stimulated lymphocytes is perhaps shifted from oxidative to glycolytic metabolism to provide additional energy for activation and proliferation [23]. In addition, three patients had elevated C-reactive protein within 5 days of the PET/CT investigation. In one previous study of patients with bacteremia by Tsai et al., it was reported that the C-reactive protein level was positively correlated with SUVavg of the spleen [24]. Thus, in the present study, elevated C-reactive protein may have produced the increase in [^{18}F] FDG uptake in the spleen observed in three patients.

In the liver, SUV was increased, but there was no difference in CT image intensity, in the patients convalescing after COVID-19 infection compared to controls. The increase in SUV indicates that the function of the liver may be dysregulated, possibly due to injury caused by SARS-CoV-2 binding angiotensin-converting enzyme 2-positive cholangiocytes, drug hepatotoxicity, or immune-mediated inflammation [11]. Impaired liver function has commonly been reported in patients with SARS, and associated with histologic findings of mild portal lymphocytic infiltration and relatively sparse lobular inflammation [25]. In the present study, only one patient had abnormal alanine aminotransferase and another abnormal aspartate aminotransferase concentration. Thus, clinically significant liver injury is relatively uncommon, even in patients with severe COVID-19 [26]. In a previous study, Lin et al. reported that alanine aminotransferase and aspartate aminotransferase were significantly positively correlated with [^{18}F] FDG uptake in the liver [27]. Thus, the raised alanine aminotransferase concentration in patient 6 and the raised aspartate aminotransferase concentration in patient 4 may be related to the increased [^{18}F] FDG uptake in the liver.

The findings of the present study suggest that increased [^{18}F] FDG uptake in the lungs and extrapulmonary sites may persist for a long period post COVID-19 infection. Scarlattei et al. reported that the metabolic activity in the lung lesions of a COVID-19 patient remained high many weeks after the symptoms disappeared and a negative RT-PCR test result [28]. This increased metabolism may be caused by the persistent presence of inflammatory cells at the site of lesions [28]. However, it is currently unclear how long the post COVID-19 inflammatory response can last in the lungs and extrapulmonary sites. Thus, further studies should be performed of the long-term metabolic activity in the lungs and other organs of patients recovering from COVID-19.

Because COVID-19 has evolved into a global pandemic, clinicians and radiologists need to have a thorough understanding of the cellular mechanisms underlying the pathophysiology of COVID-19 in different clinical settings of malignancy, infection, and inflammatory conditions and extrapulmonary sites to avoid misinterpretation of [^{18}F] FDG PET/CT imaging results. High [^{18}F] FDG uptake may be related to increased anaerobic glycolysis caused by a cascade of reactions involving inflammatory cells [29]. However, [^{18}F] FDG uptake is considered as a non-specific inflammatory or immune activation. The high [^{18}F] FDG uptake that characterized COVID-19 lung lesions is similar to the Middle East respiratory syndrome, H1N1 pandemic influenza virus, and organized pneumonia [30–32]. In addition, sometimes the lung lesions of COVID-19 may mimic tumor in PET/CT images [33]. Thus, in the midst of a COVID-19 pandemic, clinicians and radiologists have to be aware of potential misleading indications on PET/CT images. The lung lesions of COVID-19 should be differentiated from bacterial, viral, or organized pneumonia, as well as tumor [33]. Furthermore, [^{18}F] FDG PET/CT can detect inflammatory effects focusing not only on lung lesions but also on extrapulmonary sites that have been reported to be involved such as the lymph node and spleen [15].

[^{18}F] FDG PET/CT provides metabolic information, which can play a complementary role to other imaging modalities. Although [^{18}F] FDG PET/CT is currently not recommended for diagnosis of COVID-19 [34], it can add values to the challenge of diagnosing complications caused by COVID-19 [35]. In particular, [^{18}F] FDG PET/CT can be used to identify potential involvement of the lung and other organs in COVID-19 patients [36]. The information provided by [^{18}F] FDG PET/CT in patients convalescing after severe COVID-19 infection may not lead to any significant change in patient management. Nevertheless, COVID-19 can cause substantial harm in the lungs and extrapulmonary sites in a chronic setting [37]. Thus, [^{18}F] FDG PET/CT may add value in monitoring the long-term treatment outcomes in convalescing patients of severe COVID-19.

There are several limitations of the present study. First, the size of the patient cohort was relatively small. This is due in large part to the difficulty of scanning recovering patients

shortly after they have received two consecutive RT-PCR tests due to the risk of infection and the status of the patients. Second, [^{18}F] FDG PET/CT imaging was performed only once in each patient. Future studies could include recalling the subject for a second scan to obtain longitudinal data. Third, for the correlation analysis, the laboratory test to measure peripheral blood lymphocyte count was conducted within up to 5 days of the PET/CT investigation being performed. Finally, biopsy specimens were not available for the organs studied. In future studies, the relationships between imaging measurements and histopathological features of organs of patients with COVID-19 should be investigated.

In summary, inflammation-related responses remained in the lung, mediastinal lymph node, spleen, and liver of patients convalescing after severe COVID-19 infection despite two consecutive negative results of RT-PCR tests for SARS-CoV-2 nucleic acid.

Acknowledgments We thank Jianjian Cheng, Junping Liu, Hewen Wu, Huiqiang Li, Na Li, Pengyu Li, Yu Shen, Chengli Wu, Neil Roberts, and Peichun Sun for their contributions to this work.

Author contributions Guarantors of integrity of entire study: Y.B., J.X., J.G., F.S., M.W.
Study concepts and design: Y.B., J.X., L.C., C.F., J.G., F.S., M.W.
Data acquisition: W.Z., M.W.
Data analysis and interpretation: Y.B., J.X., L.C., C.F., Y.K., G.E.F., J.G., F.S., M.W.
Statistical analysis: Y.B., J.X., L.C., C.F., M.W.
Manuscript drafting: Y.B., J.X., L.C., C.F., G.E.F., J.G., F.S., M.W.
Literature research: Y.B., J.X., G.E.F., J.G., F.S., M.W.

Compliance with ethical standards

Conflict of interest The authors declare that they have no conflict of interest.

Ethical approval This study was approved by the local Research Ethics Committee.

References

1. Jacobsen KH. Will COVID-19 generate global preparedness? Lancet. 2020;395(10229):1013–4. https://doi.org/10.1016/S0140-6736(20)30559-6.
2. Guan WJ, Ni ZY, Hu Y, et al. Clinical characteristics of coronavirus disease 2019 in China. N Engl J Med. 2020. https://doi.org/10.1056/NEJMoa2002032.
3. Yang X, Yu Y, Xu J, et al. Clinical course and outcomes of critically ill patients with SARS-CoV-2 pneumonia in Wuhan, China: a single-centered, retrospective, observational study. Lancet Respir Med. 2020;S2213-2600(20):30079–5. https://doi.org/10.1016/S2213-2600(20)30079-5.
4. Bellani G, Laffey JG, Pham T, et al. Epidemiology, patterns of care, and mortality for patients with acute respiratory distress syndrome in intensive care units in 50 countries. JAMA. 2016;315(8):788–800. https://doi.org/10.1001/jama.2016.0291.
5. Chen N, Zhou M, Dong X, et al. Epidemiological and clinical characteristics of 99 cases of 2019 novel coronavirus pneumonia in Wuhan, China: a descriptive study. Lancet. 2020;395(10223):507–13. https://doi.org/10.1016/S0140-6736(20)30211-7.
6. Bai Y, Yao L, Wei T, et al. Presumed asymptomatic carrier transmission of COVID-19. JAMA. 2020. https://doi.org/10.1001/jama.2020.2565.
7. Chung M, Bernheim A, Mei X, et al. CT imaging features of 2019 novel coronavirus (2019-nCoV). Radiology. 2020;295(1):202–7. https://doi.org/10.1148/radiol.2020200230.
8. Wang D, Hu B, Hu C, et al. Clinical characteristics of 138 hospitalized patients with 2019 novel coronavirus-infected pneumonia in Wuhan, China. JAMA. 2020. https://doi.org/10.1001/jama.2020.1585.
9. Arentz M, Yim E, Klaff L, et al. Characteristics and outcomes of 21 critically ill patients with COVID-19 in Washington State. JAMA. 2020. https://doi.org/10.1001/jama.2020.4326.
10. Shi H, Han X, Jiang N, et al. Radiological findings from 81 patients with COVID-19 pneumonia in Wuhan, China: a descriptive study. Lancet Infect Dis. 2020;20(4):425–34. https://doi.org/10.1016/S1473-3099(20)30086-4.
11. Zhang C, Shi L, Wang F-S. Liver injury in COVID-19: management and challenges. Lancet Gastroenterol Hepatol. 2020;5(5):428–30. https://doi.org/10.1016/S2468-1253(20)30057-1.
12. Capitanio S, Nordin AJ, Noraini AR, Rossetti C. PET/CT in nononcological lung diseases: current applications and future perspectives. Eur Respir Rev. 2016;25(141):247–58. https://doi.org/10.1183/16000617.0051-2016.
13. Chen DL, Schiebler ML, Goo JM, van Beek EJR. PET imaging approaches for inflammatory lung diseases: current concepts and future directions. Eur J Radiol. 2017;86:371–6. https://doi.org/10.1016/j.ejrad.2016.09.014.
14. Qin C, Liu F, Yen TC, Lan X. 18F-FDG PET/CT findings of COVID-19: a series of four highly suspected cases. Eur J Nucl Med Mol Imaging. 2020;47(5):1281–6. https://doi.org/10.1007/s00259-020-04734-w.
15. Dietz M, Chironi G, Claessens YE, et al. COVID-19 pneumonia: relationship between inflammation assessed by whole-body FDG PET/CT and short-term clinical outcome. Eur J Nucl Med Mol Imaging. 2020. https://doi.org/10.1007/s00259-020-04968-8.
16. Colandrea M, Gilardi L, Travaini LL. et al, 18F-FDG PET/CT in asymptomatic patients with COVID-19: the submerged iceberg surfaces. Jpn J Radiol. 2020. https://doi.org/10.1007/s11604-020-01006-3.
17. Xu Z, Shi L, Wang Y, et al. Pathological findings of COVID-19 associated with acute respiratory distress syndrome. Lancet Respir Med. 2020;8(4):420–2. https://doi.org/10.1016/S2213-2600(20)30076-X.
18. Bellani G, Messa C, Guerra L, et al. Lungs of patients with acute respiratory distress syndrome show diffuse inflammation in normally aerated regions: a [18F]-fluoro-2-deoxy-D-glucose PET/CT study. Crit Care Med. 2009;37(7):2216–22. https://doi.org/10.1097/CCM.0b013e3181aab31f.
19. Johnson LN, Vesselle H. COVID-19 in an asymptomatic patient undergoing FDG PET/CT. Radiol Case Rep. 2020;15(10):1809–12. https://doi.org/10.1016/j.radcr.2020.07.018.
20. Mebius RE, Kraal G. Structure and function of the spleen. Nat Rev Immunol. 2005;5(8):606–16. https://doi.org/10.1038/nri1669.
21. Mathis D, Shoelson SE. Immunometabolism: an emerging frontier. Nat Rev Immunol. 2011;11(2):81. https://doi.org/10.1038/nri2922.
22. Zhan J, Deng R, Tang J, et al. The spleen as a target in severe acute respiratory syndrome. FASEB J. 2006;20(13):2321–8. https://doi.org/10.1096/fj.06-6324com.
23. Yang Z, Matteson EL, Goronzy JJ, Weyand CM. T-cell metabolism in autoimmune disease. Arthritis Res Ther. 2015;17:29. https://doi.org/10.1186/s13075-015-0542-4.

24. Tsai HY, Lee MH, Wan CH, et al. C-reactive protein levels can predict positive 18F-FDG PET/CT findings that lead to management changes in patients with bacteremia. J Microbiol Immunol Infect. 2018;51(6):839–46. https://doi.org/10.1016/j.jmii.2018.08.003.
25. Chau TN, Lee KC, Yao H, et al. SARS-associated viral hepatitis caused by a novel coronavirus: report of three cases. Hepatology. 2004;39(2):302–10. https://doi.org/10.1002/hep.20111.
26. Bangash MN, Patel J, Parekh D. COVID-19 and the liver: little cause for concern. Lancet Gastroenterol Hepatol. 2020;S2468-1253(20):30084. https://doi.org/10.1016/S2468-1253(20)30084-4.
27. Lin CY, Ding HJ, Lin T, et al. Positive correlation between serum liver enzyme levels and standard uptake values of liver on FDG-PET. Clin Imaging. 2010;34(2):109–12. https://doi.org/10.1016/j.clinimag.2009.05.007.
28. Scarlattei M, Baldari G, Silva M, et al. Unknown SARS-CoV-2 pneumonia detected by PET/CT in patients with cancer. Tumori. 2020;106(4):325–32. https://doi.org/10.1177/0300891620935983.
29. Jones HA, Marino PS, Shakur BH, Morrell NW. In vivo assessment of lung inflammatory cell activity in patients with COPD and asthma. Eur Respir J. 2003;21:567–73. https://doi.org/10.1183/09031936.03.00048502.
30. Chefer S, Thomasson D, Seidel J, et al. Modeling [(18)F]-FDG lymphoid tissue kinetics to characterize nonhuman primate immune response to Middle East respiratory syndrome-coronavirus aerosol challenge. EJNMMI Res. 2015;5(1):65. https://doi.org/10.1186/s13550-015-0143-x.
31. Jonsson CB, Camp JV, Wu A, et al. Molecular imaging reveals a progressive pulmonary inflammation in lower airways in ferrets infected with 2009 H1N1 pandemic influenza virus. PLoS One. 2012;7(7):e40094. https://doi.org/10.1371/journal.pone.0040094.
32. Alonso Sanchez J, García Prieto J, Galiana Morón A, Pilkington-Woll JP. PET/CT of COVID-19 as an organizing pneumonia. Clin Nucl Med. 2020;45(8):642–3. https://doi.org/10.1097/RLU.0000000000003174.
33. Barry O, Cabral D, Kahn JE, et al. 18-FDG pseudotumoral lesion with quick flowering to a typical lung CT COVID-19. Radiol Case Rep. 2020;15(10):1813–6. https://doi.org/10.1016/j.radcr.2020.07.035.
34. Joob B, Wiwanitkit V. 18F-FDG PET/CT and COVID-19. Eur J Nucl Med Mol Imaging. 2020;47(6):1348. https://doi.org/10.1007/s00259-020-04762-6.
35. Deng Y, Lei L, Chen Y, Zhang W. The potential added value of FDG PET/CT for COVID-19 pneumonia. Eur J Nucl Med Mol Imaging. 2020;47(7):1634–5. https://doi.org/10.1007/s00259-020-04767-1.
36. Halsey R, Priftakis D, Mackenzie S, et al. COVID-19 in the act: incidental 18F-FDG PET/CT findings in asymptomatic patients and those with symptoms not primarily correlated with COVID-19 during the United Kingdom coronavirus lockdown. Eur J Nucl Med Mol Imaging. 2020. https://doi.org/10.1007/s00259-020-04972-y.
37. Lütje S, Marinova M, Kütting D, et al. Nuclear medicine in SARS-CoV-2 pandemia: 18F-FDG-PET/CT to visualize COVID-19. Nuklearmedizin. 2020;59(3):276–80. https://doi.org/10.1055/a-1152-2341.